Kinetics of Light-Induced Concentration Patterns in Transparent Polymer Solutions

M. Anyfantakis,[†,‡,#] A. Pamvouxoglou,[†,§,∇] C. Mantzaridis,[§,∥] S. Pispas,[∥] H-J Butt,[⊥] G Fytas,[†,⊥] and B. Loppinet*,[†]

†FO. R. T. H., Institute of Electronic Structure & Laser, 71110 Heraklion Crete, Greece
‡Dept. of Chemistry, University of Crete, 71003 Heraklion, Greece
§Dept. of Material Science & Technology, University of Crete, 71003 Heraklion, Greece
∥N.H.R.F, Theoretical and Physical Chemistry Institute, 11635 Athens, Greece
⊥Max Planck Institute for Polymer Research, Ackermannweg 10, 55128 Mainz, Germany

S Supporting Information

ABSTRACT: When exposed to weak visible laser light, solutions of common polymers like poly(isoprene) and poly(butadiene) respond by local concentration variations, which in turn lead to refractive index changes. Various micropatterns have been recently reported, depending mostly on the solvent environment and the irradiation conditions. Here, we focused on the simpler case of single polymer-rich filaments and we employed phase contrast microscopy to systematically investigate the influence of laser illumination and material parameters on the kinetics of the optically induced local concentration increase in the polydiene solutions. The refractive index contrast of the formed filaments increased exponentially with the laser illumination time. The growth rate exhibited linear dependence on the laser power and increased with polymer chain length in semidilute solutions in good solvents. On the contrary, the kinetics of the formed filaments appeared to be rather insensitive to the polymer concentration. Albeit the origin of the peculiar light field-polymer concentration coupling remains yet elusive, the new phenomenology is considered necessary for the elucidation of its mechanism.
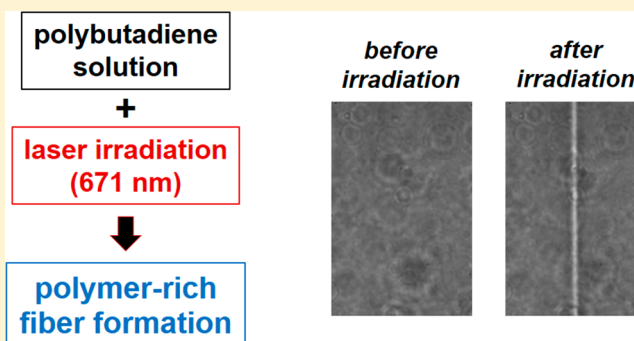
INTRODUCTION

One of the defining characteristics of soft matter is a complex response to external fields, with often spectacular nonlinearities. Most of the attention has been focused on the effect of mechanical and electrical fields.[1] Optical fields can also be used to manipulate soft matter and to trigger optical nonlinearities where light modifies the material refractive index and therefore the wave propagation.[2] In the realm of nonlinear optics, the specificity of soft matter is that nonlinearities can be attributed to mesoscopic degrees of freedom present in the material (like orientation or concentration) rather than to the electronic structure of the components as in the most common nonlinear optical materials.[3,4] As a consequence, optical nonlinearities can be present in transparent dielectric materials.

Though first quoted as artificial Kerr effect by Ashkin et al. more than 30 years ago,[5] the interest in such material has recently increased, triggered by the self-focusing possibilities offered by colloidal solutions.[2−6] Typical examples of soft matter nonlinear optics systems are nematic liquid crystals[7] and dilute colloidal suspensions.[2−6,8] Polymer blends near phase separation[9] or water-in-oil emulsions[10] have also been investigated, but there the nonlinearity was triggered by temperature gradients.[11] Fiber formation through light self-propagation has been observed and described in photoinitiated polymerization[12] in various materials including absorbing organosiloxanes.[13] In all these materials, a nonlinear self-induced focusing compensates the natural diffraction, so that light can propagate over very long distances without spreading.[14−16]
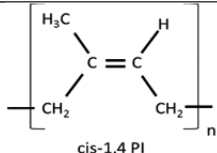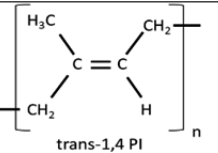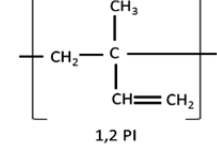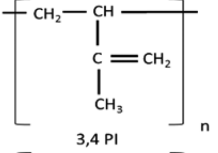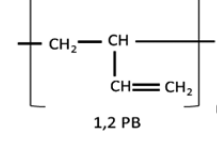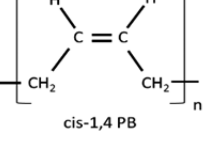
An unanticipated optically controlled soft matter manipulation and subsequent pattern formation has been reported in nondilute solutions of common polymers, such as polybutadiene and polyisoprene.[17−19] Under moderate visible laser irradiation, polymer- or solvent-rich microstructures have been observed along the direction of light propagation, depending on the solvent environment.[20] Exploiting this effect, the light-directed microfabrication of free-standing three-dimensional polydiene-based structures has been also demonstrated.[21] Despite the robust character of this peculiar effect, the origin of the light-matter coupling at work still remains unknown.

Table 1. Characteristics of the Polymers Used in This Study[a]

Name	M (kg/mol)	microstructure	
PI65	65	*cis*-1,4	
PI132	132	*cis*-1,4	
PI379	379	*cis*-1,4	
PI1091	1091	*cis*-1,4	
PI936	936	40% 1,2 and 3,4	
tPI410	410	*trans*-1,4	
PB390	390	*cis*-1,4	
1,2PB20	20	1,2	

[a]The molecular weight (M), the isomer content, as well as the chemical structure of the repeating units (monomers) are shown.

Expected optical forces[22−24] responsible for matter manipulation are too weak to account for our experimental observations. In an effort to quantify the effect, we present here a detailed study of the filament formation kinetics by *in situ* phase contrast microscopy. The influence of various parameters, including irradiation power and sample parameters, such as polymer concentration and polymer chain length, is examined. The implication of the reported results on the origin of the mechanism and its relevance for optical applications are discussed at the end of the article.

■ EXPERIMENTAL SECTION

Samples. Anionically polymerized, monodisperse poly-(isoprene) (PI) of different molecular weights (M) and 1,2-poly(butadiene) (PB), as well as commercial *trans*-1,4-PI (Sigma-Aldrich) and *cis*-1,4-PB (Polimeri Europa, Italy) (polydispersity 2.5) were used in this study. Table 1 summarizes all the polymers used here and their molecular characteristics. Typically, polydienes rich in 1,4 content contain ~92% 1,4 (mostly *cis*) units and ~8% 1,2 and 3,4 units. *trans*-1,4-PI contains ~99% *trans*-1,4 units (last column in Table 1).

The polymer solutions in different solvents were prepared by adding the desired amount of solvent to a known amount of polymer in a glass vial. Care was taken to dry the polymer in a vacuum oven for about 30 min prior to solution preparation at room temperature. All solvents were filtered through PTFE filters (pore diameters 0.2 and 0.45 μm) to avoid the presence of dust. The solutions were thoroughly stirred by a magnetic stirring bar typically for 7−10 days, to ensure fully homogeneous samples. The solutions were loaded into the sample cells using glass pipettes.

Optical Setup. The experimental setup[19] for the simultaneous pattern formation and real-time imaging of the light-induced structures is illustrated in Figure 1. A modified x-y translation stage sitting on an Axioskop 2 upright microscope (Zeiss) supported the optical elements used for irradiating the
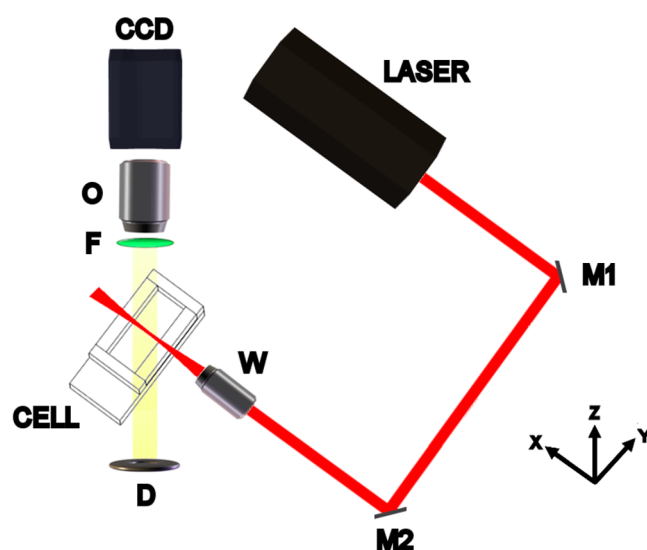

Figure 1. A schematic illustration of the experimental setup used for the irradiation and the simultaneous imaging of the polymer solutions: W, writing lens; O, microscope objective; F, movable filter to block the scattered laser light; D, microscope diaphragm and M1, M2 mirrors.

polymer solutions. These elements included the writing CW DPSS laser source (wavelength λ = 671 nm, CNI, China), a two-mirror (M1, M2) beam stirrer, and a 4× microscope lens (W, numerical aperture NA = 0.12) (Melles Griot). The focal spot (diameter~ 18 μm) was set in the middle of the sample cells along the laser beam propagation direction. Glass cells (3 mm long) with four optical windows were specially constructed to allow simultaneous laser irradiation and microscope imaging. The incident power on the sample cell was varied between 10 and 300 mW by using a stepped neutral density optical filter.

Phase contrast imaging was implemented by means of the white light Köhler illumination unit of the microscope to create
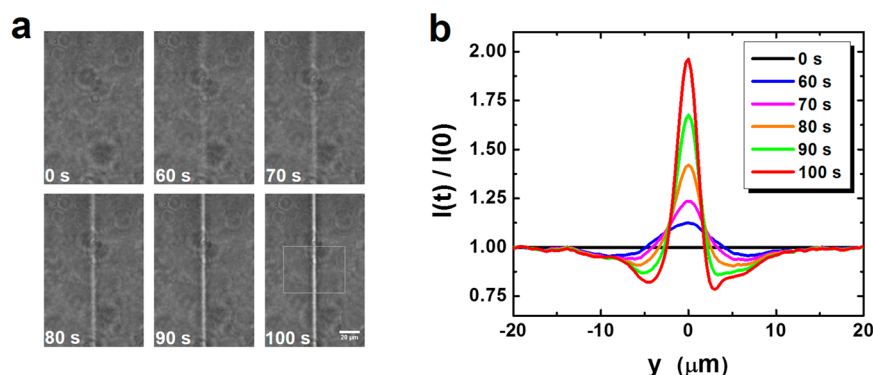
Figure 2. (a) Images of the fiber formation at different irradiation times (see also Supporting Information, Video S3). (b) Time evolution of the normalized imaged intensity profiles through the phase contrast microscopy scanned over the marked square. The sample was a PB390/tetradecane solution (c = 14.7%wt) and the laser power was P = 238 mW.

a collimated beam of a few mm, a 32× objective lens (O, Zeiss) and an 8-bit 640 × 480 CCD camera (Basler) with frame rate between 1 and 10 frames per second. The imaging was performed with a filter (F) placed in front of the CCD to block the scattered laser light. The images were acquired with the microscope objective lens slightly defocused (~20 μm above the focal plane) to permit quantitative phase contrast analysis where the intensity measured at the CCD relates to the refractive index profile.

Phase Contrast Microscopy. In order to quantify the local refractive index variation induced by the laser irradiation, we used a variant of quantitative phase contrast microscopy.[25,26] It provides an easy way to measure low refractive index change, well adapted to objects with cylindrical symmetry like the one we observed. To do so, a slightly defocused image of the pattern was acquired on a microscope using a collimated illumination. The intensity of this image can be quantitatively related to the refractive index profile of the pattern, as briefly explained below.

According to the intensity propagation formalism, the propagation of the light field with intensity I and phase ϕ along the imaging optical axis (z) obeys to the equation:[25]

$$\frac{1}{k_0}\frac{\partial I(x,y)}{\partial z} = -\vec{\nabla}(I(x,y)\vec{\nabla}\phi(x,y)) \tag{1}$$

where, $k_0 = 2\pi/\lambda$, is the wavenumber corresponding to the wavelength λ of the illumination. In our case of a feature less in-focus ($z = 0$) image $I(r, z = 0) = I_0$ and of a cylindrically symmetric pattern oriented in the x-direction eq 1 becomes

$$\frac{1}{k_0}\frac{(I/I_0)}{\Delta z} = \frac{\partial^2 \Phi}{\partial y^2} \tag{2}$$

where $I = I(x,y,\Delta z)$ is intensity imaged with a Δz defocus. The imaged intensity is directly proportional to the second derivative of the phase shift induced by the refractive index pattern. The light phase and the refractive index of the pattern are inter-related by the (inverse) Abel transform:[25]

$$k_0 n(r) = -\frac{1}{\pi}\int_r^\infty \frac{\partial \phi(y)}{\partial y}\frac{1}{\sqrt{r^2 - y^2}}\,dy \tag{3a}$$

or,

$$\phi(y) = \int_y^\infty \frac{k_0 n(r) r}{\sqrt{r^2 - y^2}}\,dr \tag{3b}$$

One can in principle quantitatively compute the refractive index profile from the measured defocused image intensities.

Here we used a simplified approach adapted to the specifics of our systems, namely a Gaussian-like shape for the refractive index pattern. For such a Gaussian functional form of the refractive index profile,

$$n(r,t) = n_0 + \delta n\exp(-r^2/a^2) \tag{4}$$

the imaged intensity $I(x,y,\Delta z)$ at a defocusing distance Δz can be calculated analytically using eqs 3b and 2,

$$\frac{1}{k_0}\frac{(I/I_0) - 1}{\Delta z} = \frac{\partial^2 \Phi}{\partial y^2} = 2a\delta n\sqrt{\pi}\frac{\partial^2(\exp(-y^2/a^2))}{\partial y^2}$$
$$= \frac{4}{a}\delta n\sqrt{\pi}\left(1 - \frac{2y^2}{a^2}\right)\exp\left(-\frac{y^2}{a^2}\right) \tag{5}$$

where we have made use of the fact that the Abel transform of a Gaussian is a Gaussian. The functional form on the right of eq 5, which is the second derivative of a Gaussian, was found to provide a correct fit of the imaged intensity profile (Figure 2b). From eq 5, the maximum of the imaged intensity, observed at the center of the pattern ($y = 0$), is directly related to the refractive index increment δn and the filament transverse dimension, a,

$$\delta n = \frac{1}{4\sqrt{\pi}}\frac{a}{\Delta z}\left(\frac{I(y=0)}{I_0} - 1\right) \tag{6}$$

Moreover in our experiments, a was observed to be independent of time, ($a(t) = a$) and hence the maximum of intensity at the center of the pattern $I(y=0)$ provided a direct measurement of the refractive index increment δn. The results are presented as $I^* = \frac{I(y=0,t)}{I_0} - 1$ versus t. The validity of this simplified approach was further assessed through a comparison with the full quantitative approach,[27] which confirmed the validity of the Gaussian profile.

The sensitivity and range of the technique as implemented here is limited by the relatively low dynamic range of the used CCD camera (8 bit). The smallest measurable intensity variation is of the order of 1% that would correspond to a refractive index change of $\delta n \sim 10^{-4}$. Alternatively, for a fiber radius $a = 5$ μm and a typical defocusing distance $\Delta z = 20$ μm, the maximum refractive index increase is estimated to be $\delta n \sim 3.5 \times 10^{-2}$. These two δn extremes imply a weight fraction
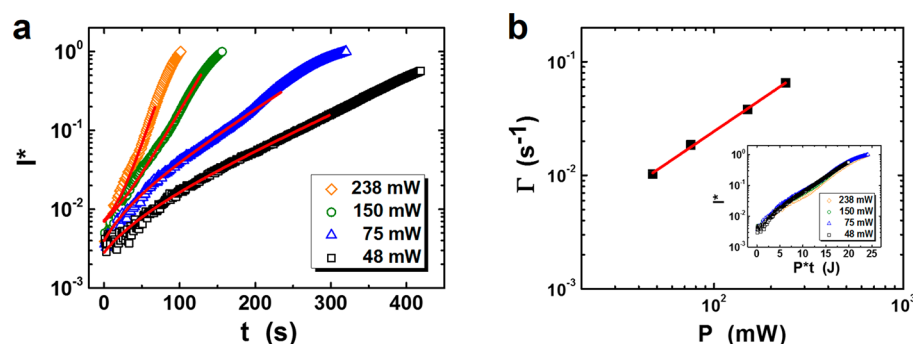
Figure 3. (a) Maximum of the normalized image intensity $I*$ as a function of irradiation time for a PB390/tetradecane solution (c = 14.7 wt%) at different laser powers, P. Solid lines indicate the representation of $I*(t)$ by eq 7. (b) Power dependence of the growth rate obtained from (pa). The red line shows a scaling relation $\Gamma \sim P^{1.1 \pm 0.1}$, the inset shows the intensity $I*$ vs the irradiation energy $P(t)$.

increase, $\delta c = \delta n/(dn/dc)$, between $\delta c_{min} \sim 8 \times 10^{-4}$ g/mL and $\delta c_{max} \sim 0.27$ g/mL, using a refractive index increment $dn/dc = 0.13$ mL/g.

RESULTS

Kinetics of the Light-Induced Refractive Index Increase. When transparent polydiene solutions were irradiated by laser light, as depicted in Figure 1, the transmitted beam (projected on a white screen) was observed to be nonsteady with an evolving concentric pattern (Supporting Information, Video S1). At the same time, the intensity of the scattered laser light (at a scattering angle of 90°) increased with irradiation time (Supporting Information, Video S2). Figure 2a shows a typical example of an observed phase contrast image sequence during laser irradiation.

Starting from a homogeneous solution with no visible pattern, a region of higher intensity (larger phase gradient) typically appeared in the image along the position of the propagating beam (Supporting Information, Video S3). As time evolved, the contrast of the imaged pattern increased. Very similar kinetics evolutions were observed in nearly all cases covering a broad range of samples and laser irradiation powers leading to the formation of a filament with robust size, but increasing refractive index. This early evolution was analyzed with the simplified quantitative phase contrast microscopy presented above and the local variation of refractive index was attributed to a local increase of polymer concentration.

Early Exponential Growth. The increase of the central intensity as a function of the irradiation time is reported in Figures 3−7. The observed growths of the normalized intensity maxima were well represented by

$$I*(t) = \frac{I(y=0, t)}{I_0} - 1 = B + A\exp(\Gamma t) \tag{7}$$

where the amplitude A, the rate Γ, and the baseline B ($\sim 10^{-3}$) accounting for small deviations at low $I*(t)$ are adjustable parameters. Other $I*$ functions including power laws (with rather high power) and compressed/stretched exponential growth could also be used, yet involving more adjustable parameters than eq 7. The growth rates returned by the exponential representation of the experimental $I*$ are displayed in Figures 3−6 for different optical and material parameters. These are the laser power P, polymer concentration c, and molecular weight M polymer−solvent refractive index difference, $\Delta n = n_p - n_0$, polymer microstructure (high and lower cis-1,4 content PI as well as trans-1,4-PI).

In a later stage, the (initially fast) evolution of the transmitted pattern was observed to slow down. The time needed to reach this later stage was found to correlate with the rate of the early growth; the faster the pattern formation at the early stage, the earlier the slowing down at the late stage. However, no clear indication of saturation of the full transmission pattern was observed as smaller secondary patterns always seemed to superimpose on the frozen primary transmission pattern. The formation of secondary structures was observed to be related to optical instabilities and in some cases to the presence of flow in the solutions.[28] The maximum refractive index increase at prolonged laser illumination (long times) obtained from the extrapolation of the recorded kinetics would correspond to a polymer fraction of the order of 0.5, i.e., significant polymer enrichment could be achieved. We next report the variation of the observed kinetics with varying the laser power and solution characteristics.

Laser Power. The influence of the laser power on the formation kinetics was examined first. The measured maximum of the normalized intensity ($I*$) for a cis-1,4-PB solution (c = 14.7 wt%) in tetradecane is shown in a semilogarithmic representation shown in Figure 3a as a function of the irradiation time t at four different values of the laser power P (Supporting Information, Figure S1 displays $I*(t)$).

The pattern formation (Figure 2a) speeds-up increasing laser power. The growth rate Γ obtained from the exponential fit of the kinetics curves (Figure 3a) is shown as a function of P in the log−log plot of Figure 3b. The solid line indicates a scaling $\Gamma \sim P^{1.1 \pm 0.1}$ relation being close to a linear dependence and is confirmed for the majority of the examined samples (Supporting Information, Figure S2). This almost linear dependence suggests the absence of multiphoton effects. It also suggests that the rate of formation at constant concentration is determined by the photon flux. The amplitude of the refractive index change is proportional to the total irradiated energy. The time-power dependence is illustrated in the inset of Figure 3, which shows the same data plotted as a function of the energy, given by the product of the laser power and the irradiation time. Interestingly, a weaker $\Gamma(P)$ than the linear dependence was observed in PB390 at very high concentrations in tetradecane (Supporting Information, Figure S3). In this case, where elastic transient gels were formed, the pattern formation is not controlled by the irradiation energy or photon flux but probably the slow material response becomes the rate-determining step.

Solvent. The variation of pattern formation kinetics for PB390 solutions in different solvents at similar concentration
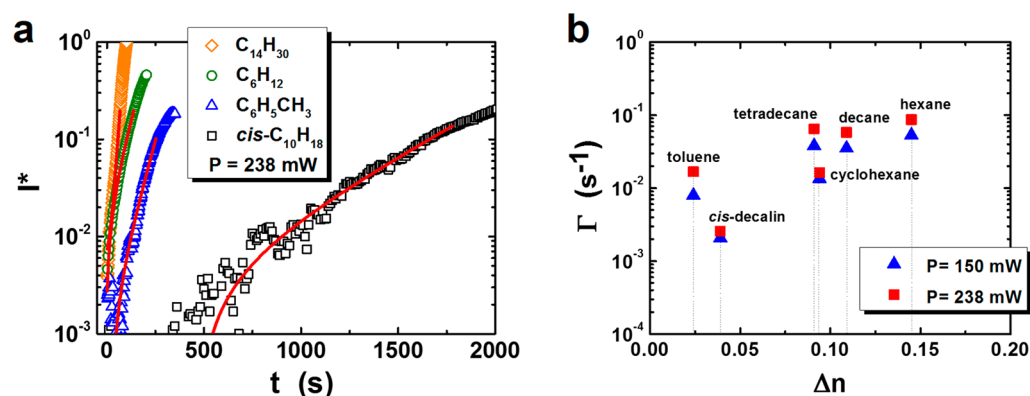
Figure 4. (a) I^* as a function of irradiation time for the same laser power ($P = 238$ mW) for cis-1,4-PB solutions in different solvents. (b) Growth fiber formation rates Γ vs refractive index difference between polymer and solvent (Δn) for a series of PB390 solutions at very similar concentrations ($c \sim 15$ wt%).
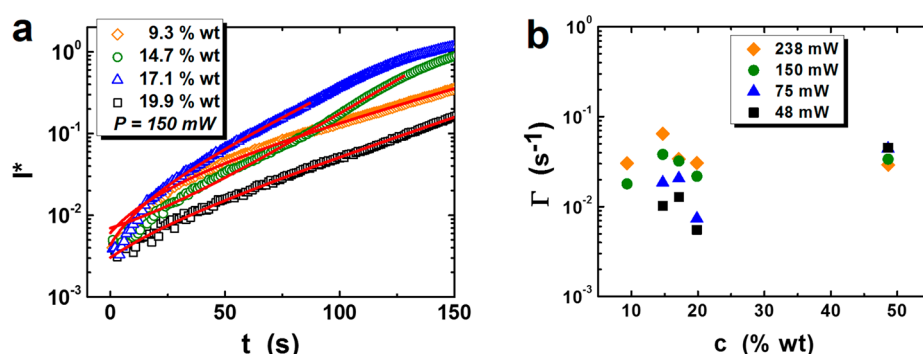

Figure 5. (a) Kinetics curves $I^*(t)$ for PB390/tetradecane solutions at different concentrations recorded at constant laser power ($P = 150$ mW). (b). Dependence of the growth rate on polymer concentration, for different laser powers.

($c \sim 15$ wt%) is presented in Figure 4. For different solvents, the increase of I^* is shown (Figure 4a) at a constant laser power. The growth rates for six different solvents are reported as a function of the optical contrast (Δn) between the polymer and the solvent for two values of the laser power in Figure 4b. The phenomenological use of Δn was motivated by a possible relation of polymer-rich pattern formation to electrostrictive forces acting on particles in colloidal dispersions.[22−24] We note, however, that the refractive index of the polymer in its bulk state is not a representative value when the polymer is surrounded by the solvent. On the contrary, for the trapping of particles by electrostrictive optical forces the utility of the solid particle refractive index is physically meaningful.

The polymer solutions in different solvents led to large variations of the growth rate. The fastest formation was observed for hexane solutions, while decane and tetradecane solutions exhibited very similar high rates, in spite of their lower Δn. A similar trend was observed for the solutions in cyclohexane and toluene. The slowest kinetics occurred in cis-decalin, being about 50 times slower than hexane. Hence, the rates reported as a function of the refractive index contrast between the polymer and the solvent do not show a clear trend. The vastly different rates in PB390/tetradecane and PB390/cyclohexane solutions is also striking, in view of the very similar solvent refractive indices. These observations prove that the refractive index increment does not exclusively control the response of these solutions to light illumination. Using the relative permittivity ε_r rather than the refractive index does not show clear trend either (Figure S4 in SI). This is in accordance with our recent observation of polymer depletion of light in a

solvent (THF) with positive Δn that excludes a solely electrostrictive mechanism.[20] The large variation of the pattern formation rate in solvents, that are otherwise very similar (viscosity, solvent quality), emphasizes the sensitivity to the specific solvent−polymer interactions.

Polymer Concentration and Molecular Weight. The role of polymer concentration c on the observed kinetics was studied using a series of cis-1,4-PB/tetradecane solutions, in the concentration range $c = 9.33−48.6$ wt%. The increase of the image intensity with illumination time along with the exponential representation at early times is shown in Figure 5a and the obtained growth rate Γ as a function of polymer concentration is shown in Figure 5b. The rate appeared to be rather insensitive to the variation of the concentration in the examined range in the semidilute regime.

Another important parameter controlling many of the polymer solutions properties is the molecular weight of the chains. In order to check the influence of molecular weight of the polymer on the formation kinetics, we compared rates obtained for PI solutions with different degree of polymerization, N. Based on previous observations, solutions of high viscosity were required to observe a strong patterning effect. Keeping concentration constant and changing molecular weight would however result in large variation of the viscoelastic properties of the polymer solutions.[29]

In an attempt to avoid too large viscoelasticity changes and possible effects on the time response, we compared solutions of various N but with different concentrations, so that the solutions display similar viscosity. To estimate the variation of viscosity, we used the scaling of viscosity with concentration
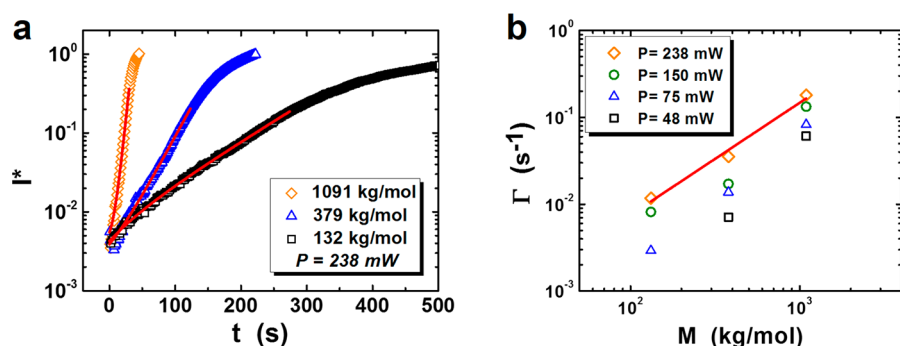
Figure 6. (a) $I^*(t)$ curves at $P = 238$ mw for three different molecular weight cis-1,4-PI solutions in decane almost equidistant from the crossover concentration, $c/c^* \geq 10$, to ensure similar viscosity. Polymer concentrations were 43.3% wt, 39.1% wt, and 5.6% wt for PI132, PI379, and PI1091, respectively. (b) Growth rate of the fiber formation in the solutions of (a) versus the PI molecular weight, M at different values of the laser power. The solid line indicates a slope of 1.3 ± 0.1 for the highest P (see also Supporting Information, Video S4).
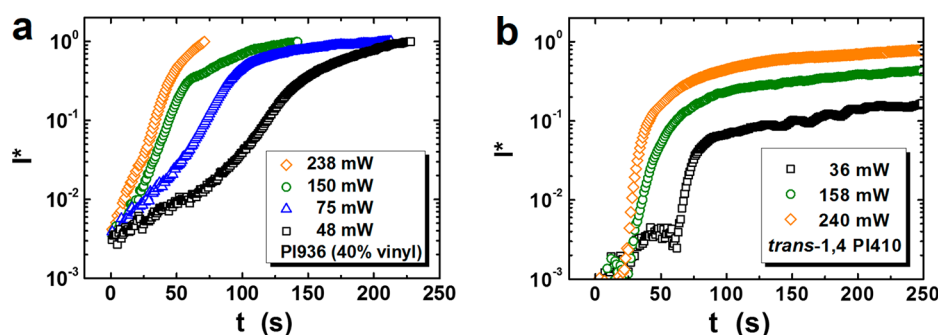

Figure 7. $I^*(t)$ curves for a 5.5 wt% PI936 (~60% 1,4 content) solution in decane in a() and 5 wt% trans-PI410 solution in toluene (b) at different values of the laser power.

and molecular weight (see SI) as $(c/c^*)^{1.3}$ where $c^* \sim N^{-0.76}$ is the overlap concentration, N is the number of monomers per chain, and the good solvent value $\nu \sim 0.588$ for the scaling exponent. To ensure high solution viscosities, the PI solutions were prepared solutions at large c/c^* ratios (≥ 10).

Figure 6a presents kinetics curves $I^*(t)$ for cis-1,4-PI solutions in decane for three different molecular weights (see Supporting Information, Video S4). Pattern growth rates as a function of polymer molecular weight M for different values of laser power are shown in Figure 6b. Under the chosen conditions, pattern formation sped up as M increased. Note that the PI decreases from 43.3% wt to 5.6% wt with increasing the molecular weight from 132 to 1092 kg/mol (to keep an almost constant c/c^*); Polyisoprene solutions with M down to 65 kg/mol also exhibited the writing phenomenon, but the weak pattern rendered quantitative measurements ambiguous. The weak effect of concentration but the rather strong influence of M is unexpected in view of the static and dynamic properties of semidilute homopolymer solutions. Increase of the viscosity and slowdown of the polymer self-diffusion as well as the increase of the osmotic pressure ($\sim \xi^{-3} \sim N^{-3\nu}$ ($c/c^*)^{-3\nu/(1-3\nu)}$ ξ being the correlation length) should reduce and oppose polymer transport to the laser focus. In the same context, the cooperative diffusion D_c is not dependent on N in semidilute regime, but only on c as $D_c \sim c^{xxx}$ and speeds-up with increasing concentration, in our case being then faster for the lower M solution as it had a larger concentration.

Polymer Microstructure. Next we examined the influence of the microstructure different compositions of 1,4- and 1,2-isoprene isomers. Mixed conformations in polydienes with controlled microstructures can be designed and accordingly

synthesized by various methods based on living polymerization.[30] In particular, various 1,4 contents can be achieved in PI through carefully chosen synthetic conditions employing mixtures of 1,2 and 3,4 units. First, we have confirmed the absence of the light effect in 1,2-PB solutions[17] also in the case of 1,2-PB ($M = 20$ kg/mol)/hexane at $c = 57.8$ wt% and $P = 300$ mW. Figure 7 presents the kinetics results for a vinyl (1,2 and 3,4) enriched PI (PI936) and trans-PI410 (see Table 1) at different laser powers.

The formation of cylindrical-like pattern was observed for the PI (PI936)/decane solution and the increase of the refractive index contrast with time expectedly sped up with the laser power (Figure 7a). When compared to the cis-PI of similar molecular weight and concentration, the PI936 (~60% 1,4) solution was overall slower and displayed an nonexponential growth. The formation kinetics in Figure 7a revealed two discernible time-regimes with the crossover transition depending on the laser power. The cylindrical-like pattern formation was also observed in a trans-PI410/toluene solution at $c = 5$ wt % and 25 °C. The shape of the image intensity is qualitatively different from the other PI solutions (Figure 6a) displayed a delayed pattern formation of a duration t_0 followed by a growth of the form $\exp\Gamma(t-t_0)$ as seen in Figure 7a. Though a clear speed up of the kinetics was observed with increasing power, the kinetics are qualitatively different from the other cis-1,4-PI solutions (Figure 6a). We note that trans-1,4 PI is highly crystalline and the solutions had to be prepared at relatively low concentration in toluene at 60 °C to facilitate dissolution.

■ DISCUSSION

An explanation for the fiber-like pattern growth and the dependence on the various examined material properties is primarily hampered by the still unknown the physical origin of this strong light−material interaction. Indeed, no simple known coupling between light and polymer concentration is expected to give rise to such a high local increase of the refractive index (Figures 3−7) in homogeneous semidilute polymer solutions with short correlation length, $\xi(c)$. Nonetheless, the main experimental findings, that can be discussed on a phenomenological base, are (i) the robust diameter for the written fiber; (ii) the exponential-like growth; (iii) the linear increase of the pattern formation rate with the laser power for all ergodic (nonelastic networks) polydiene solutions; (iv) the influence of polymer concentration, molecular weight, and solvent optical properties on the kinetics of formation, which appears to be intricate. The points (i) and (ii) can be expressed mathematically for the local change of concentration (or refractive index) as $c(r,t) = c_0[1 + \delta c_0 \exp(\Gamma t) \exp(-r^2/a^2)]$ with a rate Γ and a Gaussian-like profile with constant radius, a.

Possible Driving Forces. Propagation of light in a transparent polymer solution can be expected to give rise to optical forces with two components: (i) the gradient force oriented normal to the direction of the light propagation and with the same sign as the refractive index increment dn/dc and (ii) the scattering force oriented along the direction of propagation. They are respectively proportional to the polarizability and the square of the polarizability. In dispersions with a small characteristic size (Rayleigh regime),[23] the gradient force is the largest. In this point dipole limit the polarizability is proportional to the molecular weight (rather than to the overall volume occupied by the extended coil, as it is well-known from light scattering by polymer coils). Therefore, the force on a single polymer coil of molecular weight 10^6 g/mol (corresponding to a hydrodynamic radius of about 50 nm) will be the same than the one exerted on a pure polymer sphere with the same molecular weight (i.e., $R = 8$ nm).

The maximum attraction of the optical well[11] is given by $(2Pw_0/c_0)\ 2n\ (R/w_0)^3\ ((m^2-1)/(m^2+2))$ and can be calculated to be less than 10^{-22} J (i.e., less than kT/500) for a $R = 10$ nm radius sphere with the refractive index ration $m = n_p/n_0 = 1.1$ (n_p and n_0 are the refractive index of the polymer and the solvent, respectively), and a $P = 150$ mW laser focused to a beam radius of $w_0 = 10\ \mu$m; c_0 is the speed of light in vacuum (3×10^8 m/s). Similarly, the force exerted on such a dielectric sphere is small and of the order of 10^{-6} pN. Such a weak force is not expected to disturb the thermal equilibrium distribution. Moreover, the solution polarizability normalized by the concentration, which can be measured by light scattering experiments, is decreasing with increasing concentration and therefore it is lower in semidilute solutions compared to the dilute ones. This is a result of the ability of polymer chains to overlap leading to relatively large osmotic compressibility and therefore small characteristic dimension for concentration fluctuation ξ ($\sim R_g$ at $c \sim c^*$), combined with the relatively small refractive index increment dn/dc. Therefore, the optical forces per blob in the semidilute regime (which are expected to be proportional to the scattered intensity normalized by the concentration) should further decrease, compared to the dilute case. Finally, the nonmonotonic behavior of the pattern formation rates Γ in Figure 4b and noticeably the decoupling of the pattern

formation from the sign of the optical contrast Δn, render its relation to the gradient forces unlikely.

Temperature gradients could also be at the origin of the concentration increase through thermophoresis.[31] The low absorbance should not lead to any large temperature gradients; however, even marginal absorption may lead to small but finite temperature gradient. Interestingly, in mixtures, where no large length scales (larger than tens of nm) are present, optical forces remain weak so that thermal effects tend to dominate even in transparent mixtures.[32] For the largest power ($P \sim 300$ mW) used, a residual absorbance of about 10^{-4} cm^{-1} may lead to a temperature gradient of the order of few mK.[32] The maximum relative concentration alteration caused by thermal diffusion,[33] is $\Delta c/c = -S_T\ \Delta T$, where S_T is the Soret coefficient, characteristic of thermal diffusion. For a cis-1,4-PI/hexane solution[20] ($c = 5.02$ wt%) $S_T = 0.27$ K^{-1}, which is not expected to give rise to a concentration gradient of more than 10^{-3}. This in turn should lead to a refractive index increase $\Delta n = \Delta c(dn/dc)$, of the order of 10^{-4}, much smaller than the one observed. Moreover, the positive S_T would have driven the polymer in the cold region, away from the laser beam.

It is also worth mentioning the possibility of laser-induced chemical modification. Polydienes are known to be very sensitive to UV light and undergo photodegradation and photo-oxidation.[34] However, such effects are not expected under the used weak red light irradiation. Moreover all the solutions tested were containing small amount of antioxidant (butylated hydroxytoluene) which is expected to limit those effects. Nevertheless, local chemical modification, especially the occurrence of interchain cross-linking would lead to local change of concentration and could possibly induce self-focusing. Fiber formation through light self-propagation has been observed and described in photoinitiated polymerization in various materials.[12,13] In such systems, the induced refractive index changes followed free radical polymerization kinetics and were often saturable, i.e., $(\Delta n/\Delta n_s - 1) = \exp(-A \cdot t)$ with a saturation value Δn^s which are qualitatively different than the exponential growth of eq 7.

Another possibility for the driving mechanism is a local change of the solution thermodynamics due to the electric field gradients creating a gradient of chemical potential and thereby concentration rearrangements.[35] Such mechanism has been observed in polymer mixtures with DC field, however near to the critical point. The present polydiene solutions are in good athermal solvents and macroscopic changes are therefore unexpected.

Optical forces can also induce deformation in soft dielectric materials through the so-called Maxwell's stress, $P/c_0 w_0^2$, where c_0 is the speed of light and w_0 the beam waist.[36] Typically, deformation against elasticity is feasible for soft materials with low modulus of the order of kPa. In semidilute polymer solutions, the induced by the exciting field E dipole moment, $p_n = \alpha_n(\omega)E(r_n)$ of a nth monomer with solvent dependent polarizability $\alpha_n(\omega)$ is usually small (ω: frequency), a significant enhancement is necessary. In fact, a combined dipolar approach has been proposed for the trapping of biomolecules in solution. The observed dependence of the pattern formation on the number of monomer units in the chain (Figure 6) would be a motivation for the calculation of the total optical force considering dipoles connected in sequence.

As a final remark, it is worth noticing that the mechanisms mentioned above do not exclude each other. For example, a "seeding" mechanism (i.e., arising from a tiny local absorption

and a subsequent thermal diffusion and/or radical formation and chemical reaction) would lead to inhomogeneities giving rise to larger optical forces. This in turn would lead to a self-amplification mechanism as both optical forces F_{grad} or F_{scat} could increase during the writing process.

Pattern Radial Dimension. A striking result of the reported experiments is the robust radial dimension of the pattern, being virtually independent of the solution parameters, or the irradiation power. This size estimated by the distance between the two zero's on the x-axis in Figure 2b is smaller than the original beam dimension (18 μm fwhm). This relation is the result of the focusing and redistribution of the light by the material pattern (self-focusing) so that the Gaussian intensity distribution is compressed as the writing process proceeds. The pattern dimension reached its limited value already at the early stage of the writing effect. The constant size is even more striking as an increase of the incident light beam dimension (from ~20 μm to ~2 mm) did not lead to larger diameter fiber but to a multifiber pattern formed with all constituent fibers adopting the single fiber dimension (diameter ~10 μm).[19,28] The transverse dimension appears to be fixed by the self-focusing and rather invariable over the broad range of experimental conditions, unlike the case of photorefractive polymers.[12] This implies a local nature of the process, i.e., the pattern does not extend outside the irradiated area. A Fickian diffusion of polymer chains and solvent molecules would be anticipated to extend on a broader range and lead to nonlocal variation of the concentration.

Accelerated Exponential-like Growth Rate. We observed that the local concentration increased against the osmotic restoring force with an exponential-like time growth (e.g., Figure 3). The accelerating growth of the refractive index means that the same dose of laser irradiation leads to a larger increase of concentration as the process advances. Such mechanisms are observed in crystallization or aggregation processes in many types of materials, often described by Avrami type of equations.[37] In our case, one could imagine a light-induced aggregation mechanism leading to domain grow with increasing concentration. The growth of the domain to percolate leads to an increase of the optical forces and hence an acceleration of the process. We note that as the beam diameter is comparable to the formed pattern, we do not expect large changes of the local intensity during the pattern evolution; this amplification is at work for self-propagating at larger scale.[28]

To the best of our knowledge those type of accelerated kinetics have not been reported for light-induced changes. Instead, the reported kinetics have a constant rate of formation at the start of the process.[13] However, the kinetics of the light-induced refractive index changes have not been much addressed. The case of induced phase separation in emulsions consisting of surfactant-coated water droplets in an oil-rich continuous phase has been considered theoretically as well as experimentally, using typical phase separation description.[32] The kinetics of formation of the solid colloidal optical solitons has also been addressed, though mostly numerically.[11]

Relation to Semidilute Solutions Theory. The systems examined in this study are typical examples of semidilute polymer solutions in good solvents. Their structural and dynamic properties are well described by the semidilute solution theory providing powerful scaling arguments for quantities like the osmotic compressibility and collective diffusion through the blob model, as well as viscosity using

Rouse-reptation models.[38,39] Our findings do not seem to relate in a straightforward way to these quantities. The strong solvent dependence is not expected based on "standard" model where the effect of solvents should appear only in the dn/dc and solvent quality. Therefore, it is difficult to explain the large variation of rates in solvents of very comparable viscosities, solvent qualities and dn/dc. An association to solvent dependence is conceivable through the strength of light–matter interaction represented by the effective polarizability, $\alpha_n(\omega)$.[40] It is also difficult to relate the M and c dependence of the rate to the semidilute regime properties. We did not identify clear trends for the rate of formation as a function of the concentration c (Figure 5) beside the $c > c^*$ prerequisite for the definite observation of pattern formation. In contrast, the molecular weight seemed to control more directly the rate, since solutions of large molecular weight responded faster than solutions of lower M at constant c/c^* (Figure 6). We should expect the rate of formation and its variation with the solution characteristics to relate to the solution properties like the viscosity, diffusion coefficient and the amplitude and correlation length, ξ. The scaling of those quantities with c and M in semidilute solutions are described in the Supporting Information. Specifically, mass transport needed for the observed increase of concentration is expected to be primarily controlled by the cooperative diffusion D_c in semidilute polymer solution. In the case of association of the growth rate with D_c one would expect a molecular weight trend reverse to the one observed in Figure 6, since D_c decreases with M (at constant c/c^*). Moreover, assuming a typical value of $D_c \sim 2 \times 10^{-7} cm^2/s$ (measured by dynamic light scattering[41]) and fiber radius $a = 5$ μm, the rate $\Gamma_c \sim D_c/a^2 \sim 1$ s^{-1} appears higher than the fastest growth rate measured at the larger laser power in alkanes (Figure 4).

In conclusion, there is more at work than diffusion in semidilute solution, and probably a type of aggregation (in a broad sense, i.e., mostly irreversible local concentration increase that is induced by light) is a likely reason for the observed kinetics.

■ CONCLUSIONS

A simplified variant of phase contrast microscopy allowed for uncovering the phenomenology of the early stage kinetics of single fiber formation in polydiene solutions exposed to red laser light. We observed that with increasing irradiation time, the refractive index of the fiber increased, while its diameter remained constant. The refractive index increase followed an exponential-like behavior, for almost all solutions explored and for all irradiation powers. The exponential growth rates depended linearly on the laser power for all the samples investigated, excluding the highly viscoelastic concentrated solutions. We found that the photon flux controlled the time evolution of the refractive index increase. The precise role of various material parameters is more intricate. In particular, changing the solvent led to large variations of the kinetics of formation, so that the effective photon efficiency depends on the specific solvent–polymer couple. Similarly, the formation rate was not much affected by the monomer concentration but rather by the molecular weight of the used polymer.

Whereas the refractive index increase can safely be attributed to an increase of polymer concentration, the driving force for the local variation of polymer concentration is not yet identified. Out of the various possibilities mentioned above, none provide a fully satisfactory description even qualitatively.

So far a mechanistic interpretation of the kinetics seems to still remain out of reach.

In summary, polydiene solutions appear to provide a unique case of photorefractive polymer solution, with large induced change of refractive index (when compared to other soft/hard materials), even under mild optical conditions. This very responsive soft matter system should provide good opportunities for robust and permanent 3D (in-solution) patterning.

■ ASSOCIATED CONTENT

Ⓢ Supporting Information

The Supporting Information is available free of charge on the ACS Publications website at DOI: 10.1021/acs.jpcb.7b02239.

> Extra kinetics results; summarizing plot of the power dependence of the growth rate; and a table summarizing scaling laws of semidilute polymer solutions (PDF)
> Video of the typical evolution of the transmitted intensity pattern observed during the irradiation of a transparent semi-dilute polydiene solution with a red laser (MPG)
> Video of the typical evolution of the scattered light observed during the irradiation of a transparent semi-dilute polydiene solution with a red laser (MPG)
> Video of a series of phase contrast images obtained during the irradiation of a solution of PB390/tetradecane (MPG)
> Video of a series of phase contrast images obtained during the irradiation of a solution of PI1092/decane (MPG)

■ AUTHOR INFORMATION

Corresponding Author
*E-mail: benoit@iesl.forth.gr; Phone: +30 2810 391465;.

ORCID ⦿
M. Anyfantakis: 0000-0002-4572-5641
H-J Butt: 0000-0001-5391-2618
B. Loppinet: 0000-0003-1855-7619

Present Addresses
#Department of Chemistry, Ecole Normale Supérieure—PSL Research University, 24 rue Lhomond, 75005 Paris, France
∇Condensed Matter Physics Laboratory, Heinrich Heine University, Universitätsstr. 1, 40225 Düsseldorf, Germany

Notes
The authors declare no competing financial interest.

■ ACKNOWLEDGMENTS

■ REFERENCES

(1) Löwen, H. Colloidal Soft Matter under External Control. *J. Phys.: Condens. Matter* **2001**, *13*, R415–R432.

(2) Lee, W. M.; El-Ganainy, R.; Christodoulides, D. N.; Dholakia, K.; Wright, E. M. Nonlinear Optical Response of Colloidal Suspensions. *Opt. Express* **2009**, *17*, 10277–10289.

(3) Greenfield, E.; Nemirovsky, J.; El-Ganainy, R.; Christodoulides, D. N.; Segev, M. Shockwave Based Nonlinear Optical Manipulation in Densely Scattering Opaque Suspensions. *Opt. Express* **2013**, *21*, 23785–23802.

(4) Man, W.; Fardad, S.; Zhang, Z.; Prakash, J.; Lau, M.; Zhang, P.; Heinrich, M.; Christodoulides, D. N.; Chen, Z. Optical Nonlinearities and Enhanced Light Transmission in Soft-Matter Systems with Tunable Polarizabilities. *Phys. Rev. Lett.* **2013**, *111*, 218302.

(5) Ashkin, A.; Dziedzic, J. M.; Smith, P. W. Continuous-Wave Self-Focusing and Self-Trapping of Light in Artificial Kerr Media. *Opt. Lett.* **1982**, *7*, 276–278.

(6) Christodoulides, D. N.; Musslimani, Z. H.; Rotschild, C.; Segev, M.; El-Ganainy, R. Optical Beam Instabilities in Nonlinear Nano-suspensions. *Opt. Lett.* **2007**, *32*, 3185–3187.

(7) Peccianti, M.; Assanto, G. Nematicons. *Phys. Rep.* **2012**, *516*, 147–208.

(8) Yashin, V. E.; Chizhov, S. A.; Sabirov, R. L.; Starchikova, T. V.; Vysotina, N. V.; Rozanov, N. N.; Semenov, V. E.; Smirnov, V. A.; Fedorov, S. V. Formation of Soliton-like Light Beams in an Aqueous Suspension of Polystyrene Particles. *Opt. Spectrosc.* **2005**, *98*, 466–469.

(9) Voit, A.; Krekhov, A.; Köhler, W. Laser-Induced Structures in a Polymer Blend in the Vicinity of the Phase Boundary. *Phys. Rev. E* **2007**, *76*, 11808.

(10) Delville, J.; Lalaude, C.; Freysz, E.; Ducasse, A. Phase Separation and Droplet Nucleation Induced by an Optical Piston. *Phys. Rev. E: Stat. Phys., Plasmas, Fluids, Relat. Interdiscip. Top.* **1994**, *49*, 4145.

(11) Gordon, R.; Blakely, J. T.; Sinton, D. Particle-Optical Self-Trapping. *Phys. Rev. A: At., Mol., Opt. Phys.* **2007**, *75*, 55801.

(12) Kewitsch, A. S.; Yariv, A. Self-Focusing and Self-Trapping of Optical Beams upon Photopolymerization. *Opt. Lett.* **1996**, *21*, 24.

(13) Villafranca, A. B.; Saravanamuttu, K. An Experimental Study of the Dynamics and Temporal Evolution of Self-Trapped Laser Beams in a Photopolymerizable Organosiloxane. *J. Phys. Chem. C* **2008**, *112*, 17388–17396.

(14) Stegeman, G. I. Optical Spatial Solitons and Their Interactions: Universality and Diversity. *Science (Washington, DC, U. S.)* **1999**, *286*, 1518–1523.

(15) Segev, M. Optical Spatial Solitons. *Opt. Quantum Electron.* **1998**, *30*, 503–533.

(16) Chen, Z.; Segev, M.; Christodoulides, D. N. Optical Spatial Solitons: Historical Overview and Recent Advances. *Rep. Prog. Phys.* **2012**, *75*, 086401.

(17) Sigel, R.; Fytas, G.; Vainos, N.; Pispas, S.; Hadjichristidis, N. Pattern Formation in Homogeneous Polymer Solutions Induced by a Continuous-Wave Visible Laser. *Science* **2002**, *297*, 67–70.

(18) Loppinet, B.; Somma, E.; Vainos, N.; Fytas, G. Reversible Holographic Grating Formation in Polymer Solutions. *J. Am. Chem. Soc.* **2005**, *127*, 9678–9679.

(19) Anyfantakis, M.; Loppinet, B.; Fytas, G.; Pispas, S. Optical Spatial Solitons and Modulation Instabilities in Transparent Entangled Polymer Solutions. *Opt. Lett.* **2008**, *33*, 2839–2841.

(20) Anyfantakis, M.; Königer, A.; Pispas, S.; Köhler, W.; Butt, H.-J.; Loppinet, B.; Fytas, G. Versatile Light Actuated Matter Manipulation in Transparent Non-Dilute Polymer Solutions. *Soft Matter* **2012**, *8*, 2382–2384.

(21) Athanasekos, L.; Vasileiadis, M.; Mantzaridis, C.; Karoutsos, V. C.; Koutselas, I.; Pispas, S.; Vainos, N. A. Micro-Fabrication by Laser Radiation Forces: A Direct Route to Reversible Free-Standing Three-Dimensional Structures. *Opt. Express* **2012**, *20*, 24735.

(22) Chu, S. Laser Trapping of Neutral Particles. *Sci. Am.* **1992**, *266*, 70–76.

(23) Harada, Y.; Asakura, T. Radiation Forces on a Dielectric Sphere in the Rayleigh Scattering Regime. *Opt. Commun.* **1996**, *124*, 529–541.

(24) Novotny, L. Forces in Optical Near-Fields. In *Near-Field Optics and Surface Plasmon Polaritons*; Springer Berlin Heidelberg: Berlin, Heidelberg, pp 123–141.

(25) Barty, A.; Nugent, K. A.; Paganin, D.; Roberts, A. Quantitative Optical Phase Microscopy. *Opt. Lett.* **1998**, *23*, 817–819.

(26) Barone-Nugent, E. D.; Barty, A.; Nugent, K. A. Quantitative Phase-Amplitude Microscopy I: Optical Microscopy. *J. Microsc.* **2002**, *206*, 194–203.

(27) Papazoglou, D. G.; Tzortzakis, S. In-Line Holography for the Characterization of Ultrafast Laser Filamentation in Transparent Media. *Appl. Phys. Lett.* **2008**, *93*, 041120.

(28) Anyfantakis, M.; Fytas, G.; Mantzaridis, C.; Pispas, S.; Butt, H.-J.; Loppinet, B. Experimental Investigation of Long Time Irradiation in Polydiene Solutions: Reversibility and Instabilities. *J. Opt.* **2010**, *12*, 124013.

(29) Colby, R. H. Structure and Linear Viscoelasticity of Flexible Polymer Solutions: Comparison of Polyelectrolyte and Neutral Polymer Solutions. *Rheol. Acta* **2010**, *49*, 425−442.

(30) Hadjichristidis, N.; Iatrou, H.; Pispas, S.; Pitsikalis, M. Anionic Polymerization: High Vacuum Techniques. *J. Polym. Sci., Part A: Polym. Chem.* **2000**, *38*, 3211−3234.

(31) Duhr, S.; Braun, D. Why Molecules Move along a Temperature Gradient. *Proc. Natl. Acad. Sci. U. S. A.* **2006**, *103*, 19678−19682.

(32) Delville, J. P.; Lalaude, C.; Buil, S.; Ducasse, A. Late Stage Kinetics of a Phase Separation Induced by a Cw Laser Wave in Binary Liquid Mixtures. *Phys. Rev. E: Stat. Phys., Plasmas, Fluids, Relat. Interdiscip. Top.* **1999**, *59*, 5804−5818.

(33) Köhler, W.; Krekhov, A.; Zimmermann, W. Thermal Diffusion in Polymer Blends: Criticality and Pattern Formation. *Adv. Polym. Sci.* **2009**, *227*, 145.

(34) Piton, M.; Rivaton, A. Photooxidation of Polybutadiene at Long Wavelengths (λ > 300 Nm). *Polym. Degrad. Stab.* **1996**, *53*, 343−359.

(35) Samin, S.; Tsori, Y. Stability of Binary Mixtures in Electric Field Gradients. *J. Chem. Phys.* **2009**, *131*, 194102.

(36) Bai, R.; Suo, Z. Optomechanics of Soft Materials. *J. Appl. Mech.* **2015**, *82*, 071011.

(37) Avrami, M. Kinetics of Phase Change. I General Theory. *J. Chem. Phys.* **1939**, *7*, 1103−1112.

(38) de Gennes, P.-G. *Scaling Concepts in Polymer Physics*, 1st ed.; Cornell University Press: Ithaca, 1979.

(39) Rubinstein, M.; Colby, R. H. *Polymer Physics*, 1st ed.; Oxford University Press: New York, 2003.

(40) Minnick, M. G.; Schrag, J. L. Polymer-Solvent Interaction Effects in Oscillatory Flow Birefringence Studies of Polybutadienes and Polyisoprenes in Aroclor Solvents. *Macromolecules* **1980**, *13*, 1690−1695.

(41) Adam, M.; Fetters, L. J.; Graessley, W. W.; Witten, T. A. Concentration Dependence of Static and Dynamic Properties for Polymeric Stars in a Good Solvent. *Macromolecules* **1991**, *24*, 2434−2440.